AIAA JOURNAL
Vol. 47, No. 4, April 2009

Using Pressure- and Temperature-Sensitive Paint on the Aftbody of a Capsule Vehicle

A. Neal Watkins,* Gregory M. Buck,† Bradley D. Leighty,‡ and William E. Lipford‡
NASA Langley Research Center, Hampton, Virginia 23681
and
Donald M. Oglesby§
ATK Aerospace Company, Hampton, Virginia 23681

DOI: 10.2514/1.37258

Pressure-sensitive and temperature-sensitive paint were used to visualize and quantify the surface interactions of reaction control system jets on the aftbody of capsule reentry vehicle shapes. The first model tested was an Apollo-like configuration and was used to focus primarily on the effects of the forward facing roll and yaw jets. The second model tested was an early Orion crew module configuration blowing only out of its forward-most yaw jet, which was expected to have the most intense aerodynamic heating augmentation on the model surface. This paper will present the results from the experiments, which show that with proper system design, both pressure-sensitive and temperature-sensitive paint are effective tools for studying these types of interaction in hypersonic testing environments.

Nomenclature

$A(T)$, $B(T)$	=	temperature dependent calibration coefficients for PSP
a_{xy}	=	constants for expanded PSP calibration model
b_x	=	constants for TSP calibration model
C_h	=	convective heat transfer coefficient based on enthalpy
$C_{h\mathrm{FR}}$	=	convective heat transfer coefficient calculated using the method of Fay and Riddell
FEM	=	fluoroethylmethacrylate-isobutylmethacrylate copolymer
G_1, G_2	=	intensities obtained at the two time gates used for lifetime-based data acquisition
h_{SO}	=	low temperature enthalpy
I	=	intensity of light emitted by PSP or TSP at some pressure or temperature
I_{REF}	=	intensity at light emitted by PSP or TSP some reference pressure or temperature
$K_{\mathrm{SV}}(T)$	=	temperature dependant Stern–Volmer coefficient
P	=	surface pressure
$P_j/P_{T,2}$	=	jet pressure ratio
P_{REF}	=	reference pressure
$P_{T,2}$	=	pressure at stagnation point on the model
Pj	=	jet pressure at the RCS nozzle
T	=	absolute surface temperature
T_{REF}	=	reference temperature
T_{SO}	=	surface temperature used to calculate h_{SO}
t	=	time image was taken
t_{REF}	=	reference time for image acquisition
$Z\{\theta(T_S)\}$	=	function based on the normalized thermal parameter
β	=	substrate thermal product
β_{REF}	=	approximation of the thermal product
θ	=	normalized thermal parameter

Presented as Paper 1230 at the 46th AIAA Aerospace Sciences Meeting and Exhibit, Reno, Nevada, 7–10 January 2008; received 22 February 2008; accepted for publication 3 October 2008.

*Aerospace Technologist, Advanced Sensing and Optical Measurement Branch, Mail Stop 493. Member AIAA.
†Aerospace Technologist, Aerothermodynamics Branch, Mail Stop 408A. Member AIAA.
‡Engineering Technician, Advanced Sensing and Optical Measurement Branch, Mail Stop 493.
§Research Chemist, currently at NASA Langley Research Center, Mail Stop 493.

I. Introduction

THE accurate determination of spatially continuous pressure and temperature distributions on aerodynamic surfaces is critical for the understanding of complex flow mechanisms and for comparison with computational fluid dynamics predictions. This is especially true in hypersonic flight conditions for vehicle concepts such as reentry capsules, where complex flow phenomena such as flow transition, shock layer interactions, impinging jets, etc., often occur. Conventional pressure measurements are based on pressure taps and electronically scanned pressure transducers. Although these approaches provide accurate pressure information, pressure taps are limited to providing data at discrete points, thus making it difficult to measure surface pressures between these locations Moreover, the integration of a sufficient number of pressure taps on a surface can be time and labor intensive and expensive. Likewise, surface temperatures can be measured using discrete thermocouples or globally using infrared thermography. For discrete temperature measurements, similar limitations exist as for pressure taps while infrared thermography typically requires expensive equipment and windows that may not be readily available. Applying pressure-sensitive paint (PSP) and temperature-sensitive paint (TSP) provides alternatives for acquiring these critical global surface properties. The purpose of this work is to assess the feasibility of using PSP and TSP, and visualize and quantify the surface interaction of reaction control system (RCS) jets impinging on the aftbody surface of capsule reentry vehicle concepts. The highly complex topic of jet plume impingement on capsule reentry vehicles is beyond the scope of this paper, but is more adequately described by Buck et al. [1], and references therein.

II. Description of Measurement Techniques

A. Pressure Sensitive Paint

PSP is an optical diagnostic capable of recovering global surface pressure distributions on test models [2–6] and has been used in a variety of facilities and conditions, including hypersonic testing [7,8]. The technique exploits oxygen-sensitive luminescent

molecules that are dispersed in polymer binders, or paints. In wind-tunnel applications, the PSP is applied to the model by conventional paint spraying techniques. Light sources such as arrays of ultraviolet (UV) light emitting diodes (LEDs) are mounted external to the test section to illuminate the painted model and effect luminescence emission from the entrapped oxygen-sensitive molecules. For the majority of pressure paints, PSP emission occurs in the orange to red region of the visible spectrum ($\sim$590– $\sim$ 650 nm). The emission intensity is inversely proportional to the amount of oxygen present at the PSP surface, such that paint regions producing more emission indicate lower concentrations of oxygen relative to paint regions producing less emission. If the test gas used in the tunnel is air, the paint emission intensity can be correlated to the static pressure at the model surface, because oxygen is a fixed component in air. Charge-coupled device (CCD) cameras with spectral bandpass filters to discriminate between the excitation (UV) and emission (orange to red) signals capture the intensity image of the PSP-coated model surface, providing a means to recover global surface pressure distributions on test articles of interest. All PSP measurement systems employ a ratio of image pairs to compensate for intensity nonuniformity caused by effects other than pressure. The most significant of these are the consistency of the paint application and illumination heterogeneity.

If the test surface under study is immersed in an atmosphere containing O_2 (e.g., air), the recovered luminescence intensity can be described by the Stern–Volmer relationship [9]

$$I_0/I = 1 + K_{SV}(T)P_{O_2} \tag{1}$$

where I_0 is the luminescence intensity in the absence of O_2 (i.e., vacuum), I is the luminescence intensity at some partial pressure of oxygen P_{O2}, and $K_{SV}(T)$ is the temperature dependent Stern–Volmer constant. Because it is a practical impossibility to measure I_0 in a wind-tunnel application, a modified form of the Stern–Volmer equation is typically used. This form replaces the vacuum calibration (I_0) with a reference standard [4]

$$I_{REF}/I = A(T) + B(T) \times (P/P_{REF}) \tag{2}$$

where I_{REF} is the measured luminescence intensity at a reference pressure, P_{REF}. $A(T)$ and $B(T)$ are temperature dependent constants for a given PSP formulation and are usually determined beforehand using laboratory calibration procedures.

There are two methods for acquiring PSP data. The most common method used for data acquisition is an "intensity-based" technique. During intensity-based PSP experiments, I_{REF} is typically acquired while the wind tunnel is off or at very low speed, and P_{REF} is the static pressure when no wind is applied. Thus I_{REF} is referred to as the "wind-off" intensity. I is the recovered luminescence intensity at some pressure P. Because these data are collected at a specific condition in the wind tunnel, I is also referred to as the "wind-on" intensity.

A second method of PSP data acquisition is known as "lifetime-based" PSP [10–14]. In the lifetime-based technique, excitation of the PSP is accomplished using a modulated light source (e.g., laser, flash lamp, or pulsed LED arrays). A fast framing camera (intensified CCD or interline transfer CCD) is used to collect the excited-state luminescence decay. Typically the decay is approximated by acquiring two or more images at different delay times during and/or after the pulsed excitation and integrating photons for fixed periods of time (i.e., gate widths) that have been predetermined to maximize the pressure sensitivity, as demonstrated in Fig. 1. The first image (gate 1) usually consists of a short gate width and is collected either during the excitation pulse or shortly after it ends. This can be thought of as the reference image because the excited-state decay has the least pressure sensitivity. The second image (gate 2) typically has an equal or longer gate width than gate 1, but is taken at a later time after the excitation pulse, ensuring maximum pressure (and temperature) sensitivity.

The lifetime method was chosen for the PSP portion of the test because all data are taken at the run conditions. The facility that was used for the investigations uses a model injection system in which the model is held in a separate chamber until ready for use. Once the airflow in the test section is established and consistent, the model is then injected into the flow. To use the standard intensity-based data acquisition technique, a reference image would need to be acquired at wind-off conditions; however, taking all data at the run condition can greatly reduce temperature changes between the reference and run images (gates 1 and 2). For the pressure changes expected on the models for this test, any large temperature difference between the reference and run images could overwhelm changes due to pressure.

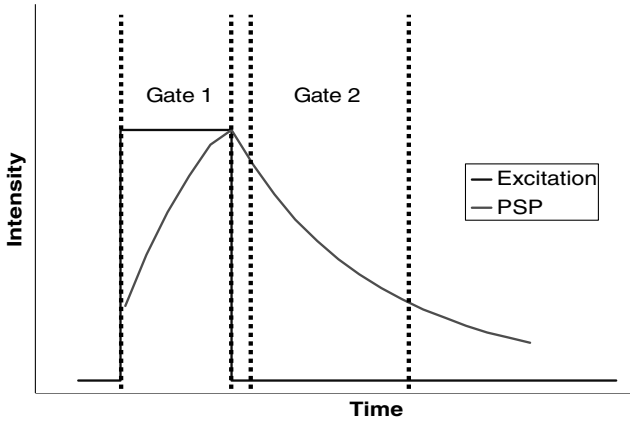

Fig. 1 Schematic representation of lifetime-based data acquisition showing excitation (blue) and measured emission (red). The gate regions represent example gate 1 (during excitation) and gate 2 (after excitation).

B. Temperature-Sensitive Paint

Global surface heat transfer measurements have been widely reported at NASA Langley Research Center (LaRC) using such techniques as thermographic phosphor coatings [15–17] and infrared thermography [18]. However, these techniques suffer from some limitations. The current thermographic phosphor coatings used at LaRC generally require models to be made from silica ceramic materials, require UV illumination (below 375 nm), and are more suited for higher temperature ranges exhibited on a heat shield than on an aftbody. Infrared thermography suffers from limitations mentioned above, specifically expensive specialized equipment such as cameras and window materials. These techniques have been used in a variety of heat transfer measurements and transition detection experiments at speed regimes from subsonic to hypersonic and at various testing temperature ranges (from cryogenic to room temperature and above) [5–7,15–17,19–24].

TSP is analogous to PSP except that the luminescent molecules are chosen for maximum temperature sensitivity (as opposed to minimal for PSP) and are dispersed in an oxygen *impermeable* binder to limit quenching by oxygen. Thus all quenching occurs through nonradiative temperature effects. In this regard, TSP and thermographic phosphor coatings are similar techniques and use many of the same data acquisition and analysis procedures. However, thermographic phosphors have generally been designed to work at higher temperatures, thus precluding the use of larger molecules which accept near UV to visible excitation or polymer binders for application. Typical thermographic phosphor materials are insoluble and thus need to be suspended in an applicable ceramic binder. This typically results in coatings that exhibit aggregation of phosphor molecules (resulting in "graininess" of the images at high spatial resolutions). For TSP applications, judicious selection of the luminophore molecule can allow excitation to be accomplished using near UV to blue light, as well as the formation of homogeneous coatings as the luminophore can be dissolved to form a more traditional paintlike coating. Data acquisition techniques for TSP are the same as for PSP. For this work it was necessary to acquire a large amount of data in a short time frame, so a standard intensity-based data acquisition technique was chosen, in which a wind-off reference image is used with a number of wind-on images to calculate surface temperatures.

III. Experimental

A. Paint Formulations

The PSP formulation used for this study was based on a formulation developed at NASA LaRC and described previously [25]. The oxygen-permeable layer is made from a copolymer of trifluoroethylmethacrylate and isobutylmethacrylate (abbreviated FEM), in which platinum meso-tetra(pentafluorophenyl)porphine is dissolved. Before application to the model, the surface was first cleaned and degreased using acetone. After drying, a white acrylic primer was applied to the surface to act as a base coat to enhance adhesion of the FEM top coat as well as to enhance scattering of the luminescence intensity back to the camera.

The TSP formulation used was also based on a formulation developed at NASA LaRC. In this case, the oxygen impermeable layer is a commercially available clear urethane sealant in which the luminophore ruthenium tris-bypyridine is dissolved. This was applied over the same base coat as the PSP.

B. Paint Calibration

All paint calibrations were performed separate from the wind tunnel in a laboratory calibration chamber. A PSP or TSP formulation was applied to 3-in.-diam aluminum coupons at the same time that all model pieces were being painted. These coupons were then placed in the calibration chamber and the luminescence intensity was measured at varying temperatures and pressures (for PSP) or varying temperatures (for TSP).

The current calibration chamber cannot reach the extremely low pressures needed to adequately calibrate the PSP formulation for hypersonic applications (typical test section pressures are on the order of 0.07 kPa or less). To account for this, an oxygen standard was used instead of regular air for calibration. This is a viable technique used to calibrate PSP for cryogenic conditions (in which small amounts of oxygen are injected into a high-pressure nitrogen flow) [26–28] and it works because the PSP is actually an oxygen sensor and is not readily affected by the actual gas pressure. To simulate the expected pressure range, a mixture of 2081 ppm (±2%, certificate of analysis) oxygen in nitrogen was used for calibration, leading to an effective calibration pressure range of 0.0007 to 1 kPa (assuming air is 21% oxygen, or 210,000 ppm, this effectively decreases the measured pressure by 100). The paint formulation was calibrated over these pressure ranges at temperatures ranging from 294 to 338 K. The lifetime technique was used to calibrate the paint, with gate 1 occurring from 0–30 μs (the width of the excitation pulse) and gate 2 occurring from 35–85 μs (5 μs after the end of the excitation pulse), and the results are shown in Fig. 2. A calibration model for the coating was derived by solving Eq. (2) for pressure in terms of the temperature and gate intensities. The calibration data showed a multidimensional dependence on both pressure and temperature, which can be attributed to the complex nature of oxygen diffusion into the polymer binder [4–6]. A linear least squares algorithm was used to fit the data to a modified and expanded version of Eq. (2) above assuming a second order relationship in both temperature and pressure

$$P = (a_{11} + a_{12}T + a_{13}T^2) + (a_{21} + a_{22}T + a_{23}T^2)(G_1/G_2) + (a_{31} + a_{32}T + a_{33}T^2)(G_1/G_2)^2 \quad (3)$$

where P is the pressure, T is the absolute temperature, G_1 and G_2 are the intensities in the respective gates (analogous to I_{REF} $[G_1]$ and $I[G_2]$), and a_{xy} are the calibration coefficients.

For TSP calibrations, the chamber was set to a constant pressure and the temperature increased from 273 K to illuminating the coupon and the results are shown in Fig. 3. Several different pressures were examined and the paint showed essentially no sensitivity to oxygen (unable to be measured). For this range of temperatures, the data most closely fit an inverse third order model

$$T/T_{\mathrm{REF}} = b_1 + b_2/(I_{\mathrm{REF}}/I) + b_3/(I_{\mathrm{REF}}/I)^2 + b_4/(I_{\mathrm{REF}}/I)^3 \quad (4)$$

where T is the temperature, T_{REF} is the reference (wind-off) temperature, I and I_{REF} are the respective image intensities, and b_x are the calibration coefficients. To compare the TSP formulation with the LaRC thermographic phosphor formulation, the relative temperature sensitivity was calculated as follows [29]:

$$\text{relative temperature sensitivity } (\%/\mathrm{K}) = \left(\frac{\mathrm{d}I(T)}{\mathrm{d}T}\right) * \frac{1}{I(T)} \times 100 \quad (5)$$

For the thermographic phosphor formulation, the sensitivity was calculated using the weighted logarithmic difference between the two color phosphors, as explained in more detail by Merski [17]. The comparison of the sensitivities of the two coatings is shown in Fig. 4. Although the TSP shows greater sensitivity over its entire range, it should be noted that the intensity of the TSP formulation is almost nonexistent at temperatures greater than 350 K whereas the thermographic phosphor produces adequate intensity to temperatures in excess of 440 K.

C. Experimental Setup

All model testing was performed in the NASA LaRC 31-in. Mach 10 wind-tunnel facility, which has been described in detail previously [30]. The 31-in. Mach 10 facility consists of high-pressure air storage rated to a maximum pressure of 30 MPa, a 12.5-MW electrical bundle heater that heats the air to approximately 1000 K, a settling chamber, a three-dimensional contoured nozzle, a test section, adjustable second minimum, after-cooler, vacuum spheres, and vacuum pumps. A 5-μm in-line filter, before the nozzle, removes particles from the airflow that can damage the ceramic

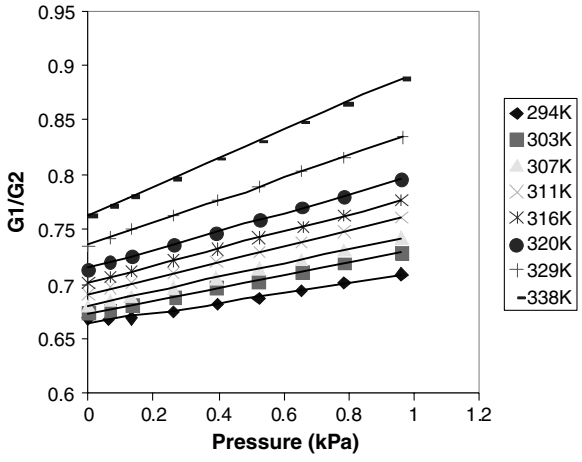

Fig. 2 G1/G2 values for PSP formulation at various pressures and temperatures.

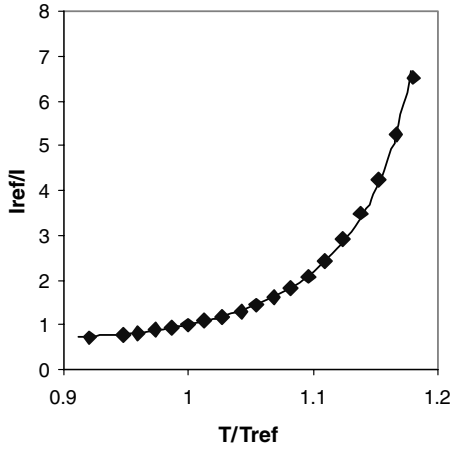

Fig. 3 Calibration data for the TSP formulation. The line through the points is the fit to Eq. (4).

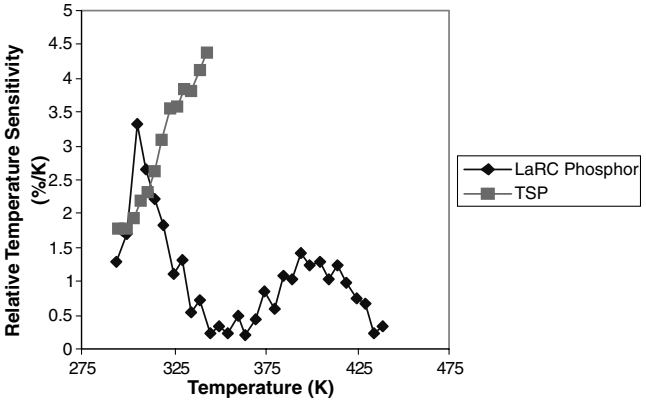

Fig. 4 Comparison of the relative temperature sensitivities for the TSP formulation and a representative LaRC thermographic phosphor coating.

phosphor models. The nozzle itself has a 2.7-cm-square beryllium copper throat, and its exit height is 0.7874 m. The test section has a 0.75 m × 0.45 m tempered-glass window for optical experimental techniques. Wind-tunnel models are protected from the flow as the tunnel comes to its operating condition by a door in the side wall of the test section. After the operating condition is reached, the model is injected to the tunnel centerline in approximately 0.55 s from the back side of the test section using a hydraulic injection system. Freestream Reynolds numbers obtained in this tunnel vary from 1.5×10^6/m to 6.5×10^6/m, and the average speed of the tunnel was Mach 9.58 ± 0.2.

A detailed description of the models used for this test is described elsewhere [1]. The models were constructed with a steel fore-body heat shield and plastic/ceramic nanocomposite aft bodies. Two distinct aftbody shapes were studied. The first shape mimicked an Apollo-era design that had no protrusions whereas the second shape was based on an early NASA Orion design (under the Constellation program). In addition to the aftbody shapes, several different RCS jet configuration pieces were also constructed to provide flexibility in experimental design. A collection of the pieces is shown in Fig. 5. Because the nanocomposite material used for the aft bodies is an insulating material, the model for PSP was coated with an additional thin layer of copper (∼635 μm thick) to dissipate heat and provide a surface with near uniform temperature. In addition, three pressure taps were available to calibrate and correlate PSP results. The models were 127 mm in diameter with an angle of attack set at 24 deg. Each RCS jet had a 685-μm-diam throat and an exit area to throat ratio of 22.5. The RCS jet chamber pressures were set at either 1725 or 3450 kPa, and were set before injection so that the jet is firing as the model is injected into the tunnel.

The lifetime technique was used to collect all PSP data to minimize the slight inconsistencies in sting positioning as well as the significant differences in reference temperature and pressure.

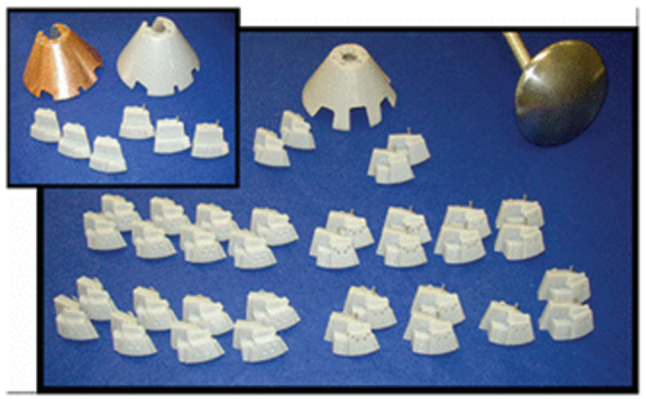

Fig. 5 Aftbody pieces for the Apollo-era (inset) and Orion-derived model shapes including various RCS jet configurations.

Illumination was provided using four LED-based arrays. The LEDs that make up the arrays have a center wavelength of 400 nm, and the arrays are capable of high pulse rate operation. The arrays were pulsed for 30 μs at a rate of 1667 Hz to acquire all data. Images were acquired using an interline transfer camera that was modified to allow "on chip" accumulation of multiple images. The camera has an array size of 1392 × 1040 pixels and 12-bit digitization. The camera is thermoelectrically cooled to minimize shot noise. To further maximize collection efficiency, the camera's CCD array was binned by a factor of 2 both horizontally and vertically (resulting image sizes are 696 × 520 pixels). The gate widths and delays are described in the calibration section above. To minimize time on the centerline, only one image was acquired (using 750 LED pulses) at each gate. This resulted in a data acquisition time (both gates) to ∼3 s, resulting in little heating as measured by embedded thermocouples.

TSP data were acquired using a standard intensity-based method. In this mode, the LED arrays were run in a continuous fashion and images were acquired using a noninterline transfer camera. This camera has an array size of 1600 × 1200 pixels and 14-bit digitization and is thermoelectrically cooled. The camera was also binned to increase collection efficiency (image sizes are 800 × 600 pixels). The reference image was acquired by injecting the model into the test section before tunnel operation. The model was then retracted into the model box, and the tunnel started. Once tunnel conditions stabilized, the model was reinjected and data collection began. TSP images were acquired every 400 ms throughout the run, lasting 10 s while the model was in the tunnel on centerline.

D. Data Analysis

Analysis of the PSP images involved ratioing gate 1 to gate 2 and applying the calibration determined in the external calibration chamber. However, this typically resulted in a bias in the recovered pressures when compared with the taps on the model. This bias was due to small systematic errors, such as slight differences in paint application between the calibration coupon and the actual model, as well as gradients in the measured temperatures on the model. To account for this, the pressure taps were used to calculate a scaling factor that was then applied to the data. This only served to change the offset of the recovered pressures values from the PSP. It did not change the calibrated PSP pressure sensitivity. Using this technique, the PSP data typically agreed with the pressure taps to within 10%. A representative slice through the pressure taps showing the agreement between the PSP and the taps is shown in Fig. 6.

Analysis of the TSP images involved an additional step. As the reference image was acquired before the operation of the tunnel, a slight misalignment was seen between the wind-off and wind-on images. Dark fiducial marks were placed on the painted surface to act as targets to aid in registration of the images. Once the position of

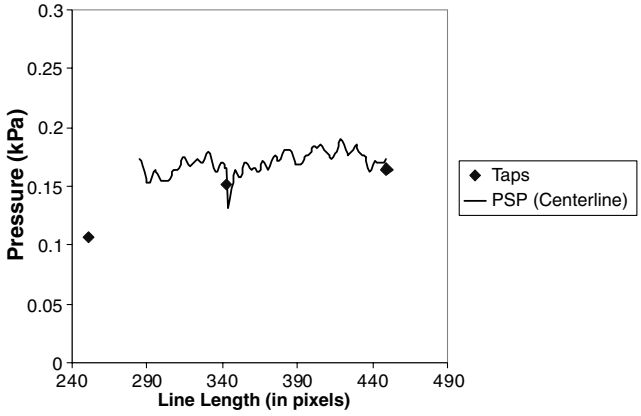

Fig. 6 A comparison of the results obtained from PSP with the measured pressures from the pressure taps. The first pressure tap was not included in the analysis as it was next to the jet exit and no suitable PSP data could be extracted from this region.

each mark was determined in each image, a second order polynomial was used to correlate the images and allow for further processing. Once correlated, the reference image was ratioed with the run image and the TSP calibration was applied. The temperature data were then used to calculate the convective heat transfer coefficient using the following relation (derived from the step solution to a one-dimensional semi-infinite slab heat transfer model [31])

$$(C_h/C_{h\mathrm{FR}})(\beta_{\mathrm{REF}}/\beta) = Z\{\theta(T_S)\}(\beta_{\mathrm{REF}}/C_{h\mathrm{FR}}) \times (T_{SO}/h_{SO})(t - t_{\mathrm{REF}})^{-1/2} \quad (6)$$

where C_h is the convective heat transfer coefficient based on enthalpy, $C_{h\mathrm{FR}}$ is the convective heat transfer coefficient calculated using the method of Fay and Riddell [32], β is the substrate thermal product, β_{REF} is an approximation for the thermal product, $Z\{\theta(T_S)\}$ is a function based on the normalized thermal parameter θ, T_{SO} is the surface temperature used for calculating low temperature enthalpy (h_{SO}) using the GASPROPS code [33], and t and t_{REF} are the image time and initial reference time, respectively. For this test, the exact value of the substrate thermal product β was unknown for the stereolithography material, so the heating results are presented as $C_h/C_{h\mathrm{FR}}$ multiplied by $\beta_{\mathrm{REF}}/\beta$ to acknowledge a factor of error. Once the temperature maps are converted to heating coefficients, the augmentation effect from the RCS jets can then be directly calculated by comparing the heating with a jet firing to the same condition without the jet firing. This measurement of heating augmentation should be unaffected by the substrate thermal product and paint as it is canceled in the ratio.

The jet pressure ratio, $P_j/P_{T,2}$, is defined as the ratio of the pressure of the RCS nozzle to the pressure at the stagnation point on the model. This provides a nondimensional method to compare the RCS performance at different Reynolds numbers and jet blowing pressures. This was also the method used previously to determine jet effectiveness [30], thus providing a way to compare current results with historical results.

IV. Results and Discussion

A. PSP Results

The initial focus of this work was to assess the viability of using PSP to measure the pressure changes on the aftbody surface of a capsule reentry vehicle due to the firing of an RCS jet. Toward this goal, all PSP work was performed on an Apollo-era design, due to its simplicity as well as the existence of heating data taken previously on these types of configurations. The Apollo design was also the only aftbody to be coated with copper. The effects of coating the aftbody with copper are shown in Fig. 7. This is a comparison of readings from an embedded thermocouple on an aftbody with and without the copper coating as well as the reading from the position sensor. When the position sensor reading is near zero, the model is fully injected into the tunnel. From these data it is clear that the presence of the copper coating serves to mitigate the temperature rise on the surface while the model is injected. The overall temperature change was approximately 0.3 K with copper and approximately 2.5 K without copper, corresponding to pressure errors of ~10%. The copper coating would eventually heat to a larger extent than the bare model, but this would occur well after the model was removed from the flow. After a run, the model was allowed to cool to room temperature by removing it from the model box while the tunnel was reset for the next run.

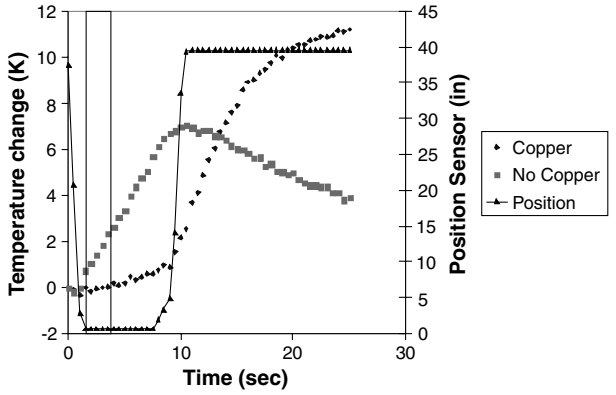

Fig. 7 Comparison of the temperature change on the aftbody with and without the copper coating. The data acquisition window is shown by the vertical lines.

PSP results from the yaw RCS jet at several Reynolds numbers and jet blowing pressures are shown in Fig. 8. It should be noted that the noise in the data is mostly due to photon shot noise as the pressure regime being investigated is approaching the practical limit of the PSP formulation, as evidenced in the calibration data shown in Fig. 2. The effects on the surface are clearly visible in all of the cases, with the greatest effects occurring at the highest Reynolds number and blowing pressures, which corresponds to the higher $P_j/P_{T,2}$ values. The pressure scale was expanded to negative values to facilitate viewing of the jet effects on the surface. This is more evident when a slice of pressure data is taken near the yaw jet as depicted in Fig. 9. These data show that there is a definite increase in surface pressure due to increasing the jet pressure, but this effect is very small. However, as seen in Fig. 8, it is also apparent that the surface effect from the yaw jet is highly dependent on the jet pressure ratio. Visual inspection shows that when the jet pressure is low ($P_j = 1725$ kPa), "augmentation" (or jet effect relative to no jet blowing) seems greatest (though only slightly) at the lowest Reynolds number ($Re = 2.6 \times 10^6$/m), but as the jet pressure is increased, the greatest augmentation is seen at the higher Reynolds number. Finally, it also illustrates that these measurements suffer from a large amount of noise as this is nearing the practical limits of PSP technology. This could possibly be extended by taking significantly more data; however, this was precluded in this facility due to excessive heating that would be experienced with increased run time.

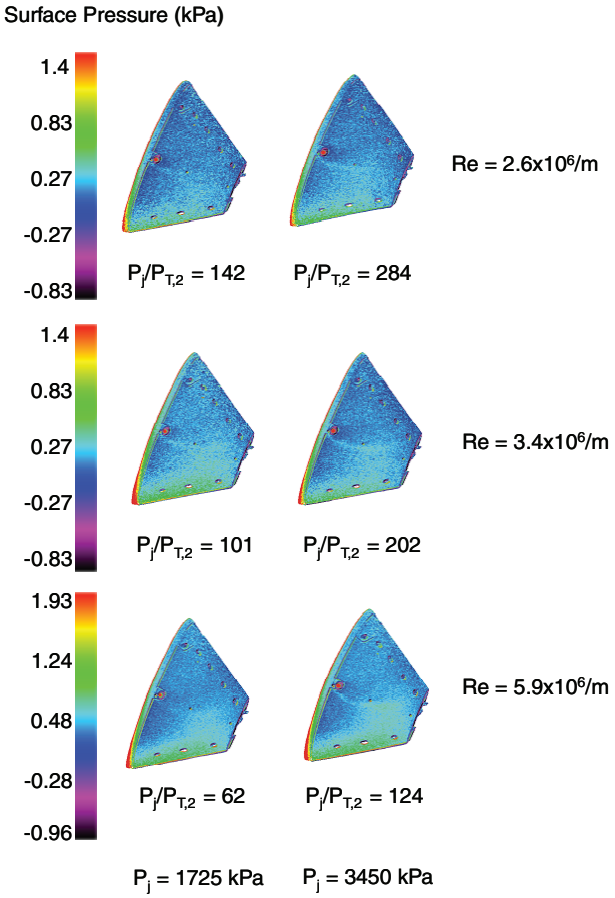

Fig. 8 PSP results from the Apollo configuration at increasing Reynolds number (Re) and different RCS yaw jet blowing pressure (P_j).

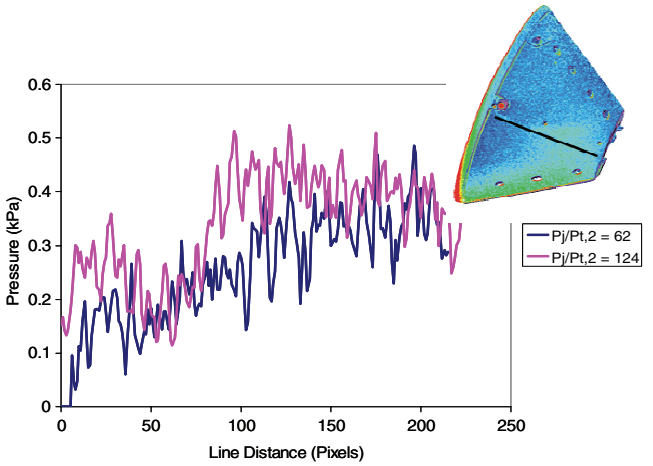

Fig. 9 Line cut of PSP data recovered for the Apollo configuration at $Re = 5.9 \times 10^6$/m at different yaw jet blowing pressures. The line in the inset shows the approximate location of the cut.

From previous thermal measurements on RCS jet interactions for this model shape [34], a greater pressure response should be seen when the roll RCS jet is employed. This result was confirmed as shown in Fig. 10. Furthermore, visual inspection of the images shows that the greatest augmentation effect is seen at the largest Reynolds number and highest jet blowing pressure. In fact, as the jet pressure ratio is lowered, the augmentation effect actually increases. These results qualitatively agree with results derived from Jones and Hunt using phase-change paints [34]. Representative pressure slices through the jet region (similar to Fig. 4) are shown in Fig. 11 and confirm the higher pressure response including greater signal to noise compared with the yaw jet.

B. TSP Results

TSP was used to visualize and quantify the heating effects of the RCS jet interaction to assess its capability for use in hypersonic test facilities. In this experiment, the overall temperature changes on the aftbody should be significantly lower than on the heat shield and

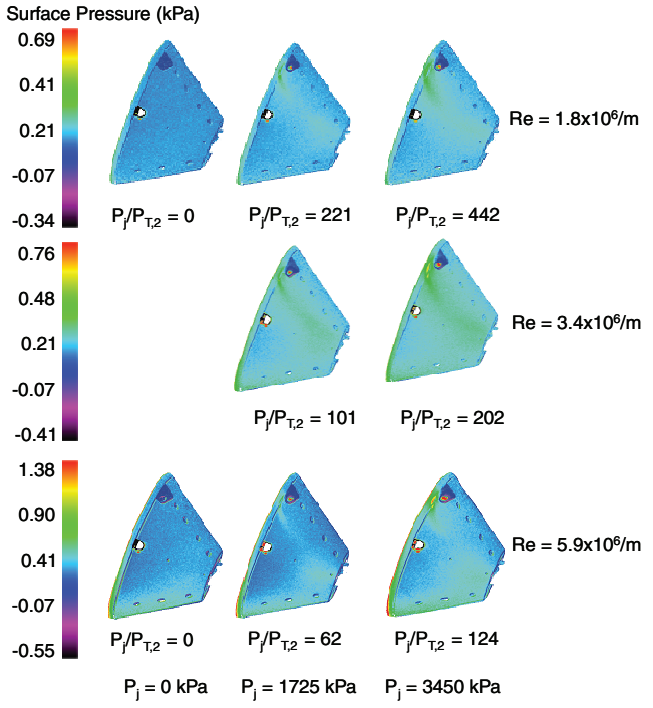

Fig. 10 PSP results from the Apollo configuration at increasing Reynolds number and different RCS roll jet blowing pressure.

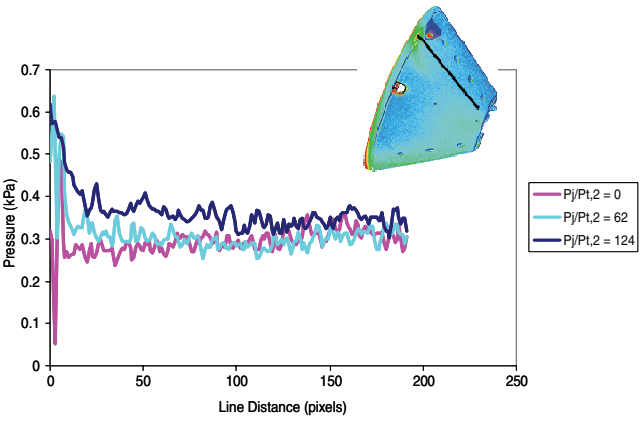

Fig. 11 Line cut of PSP data recovered for the Apollo configuration at $Re = 5.9 \times 10^6$/m at different roll jet blowing pressures. The line in the inset shows the approximate location of the cut.

approaching the lower limit of the existing thermographic phosphor technique currently used. The temperature changes observed on the aftbody of the model are well within the operating range of the TSP used and exhibit better sensitivity than the existing thermographic phosphor coatings. All TSP measurements were performed on aftbody shapes that were not coated with copper as the nanocomposite material is a good insulator, constraining most if

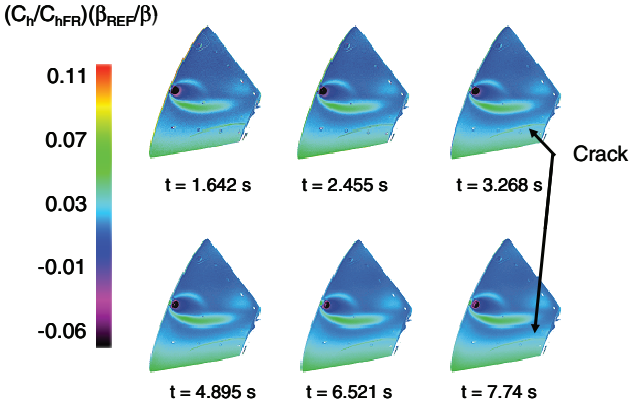

Fig. 12 Representative heating images recovered using TSP on the Apollo configuration at $Re = 0.56 \times 10^6$ and yaw jet blowing pressure of 3450 kPa. The location of the thin crack is also depicted.

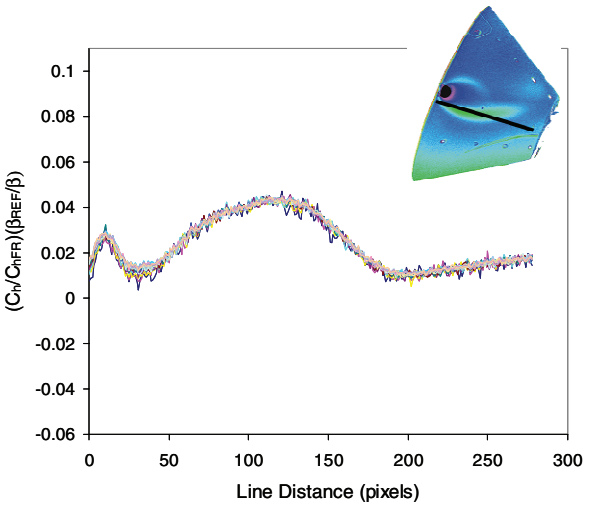

Fig. 13 Heating data calculated throughout an entire run. Tunnel conditions are the same as in Fig. 12. The inset shows the approximate location of the slice.

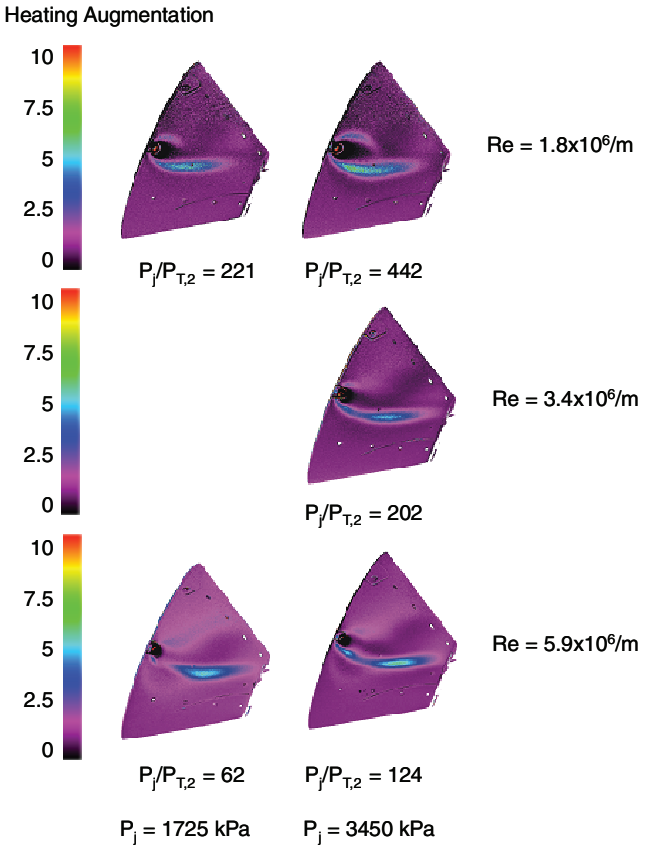

Fig. 14 Heating augmentation factors calculated for yaw jet firing on the Apollo configuration.

not all of the temperature changes to the surface. A thin, long crack occurred in the TSP coated aftbody during installation of the yaw jet (seen on the lower portion of the model at the yaw jet conditions and labeled in Fig. 12), but all jet interactions occur away from this defect, so its effects were ignored. In addition, the steel forebody was previously painted with PSP, and because the emission of the PSP is in a different part of the visible spectrum than the TSP (650 nm for the PSP compared to 600 nm for the TSP), the spectral filtering on the camera precluded any visualization of this piece.

To determine if TSP is a viable technique, data from one of the test conditions were compared to ensure that the calculated heating results did not vary appreciably during a given run. This has been shown to be the case using the thermographic phosphor coatings and should hold for TSP as well. Figure 12 depicts several heating images calculated at various times during a run. It also shows the effects of the adiabatic expansion of the gas as the actual jet exit is very dark, corresponding to low temperature. Currently, there is no capability to eject a heated flow stream from the jet, which should alleviate this effect. Visually, all of the images show essentially the same results, and this is further demonstrated if a cut of the heating data is compared for all of the images of the run, as shown in Fig. 13. Disregarding the noise at the beginning of the run (where temperature changes are quite small), the calculated heating values are the same.

To quantify the effects of the jet on the surface, a heating augmentation term is defined as the ratio of the heating calculated with the jet on to the heating calculated with the jet off. Using this definition, Fig. 14 shows the heating augmentation effects from the RCS yaw jet interaction on the Apollo aftbody. As opposed to the PSP data above, the interactions are quite clear and show some interesting phenomena. There is also a shock interaction at the jet that is most prevalent at the higher $P_j/P_{T,2}$ values. In addition, as the $P_j/P_{T,2}$ value increases, the heating augmentation tends to "broaden" but the overall heating augmentation factor is relatively constant. This is also evident when slices of the heating augmentation factors are taken near the jet, as shown in Fig. 15. These data show that the overall heating augmentation for the yaw jet is about 5–6. Physically, this means the capsule experiences an increase in heating by a factor of 5 to 6 in regions where the jet interacts with the surface compared to heating rates when the jet is not being fired. The "broadening" effect of the jet as $P_j/P_{T,2}$ can be seen as the peak heating augmentation is seen farther from the jet at lower $P_j/P_{T,2}$ (Fig. 15a), which moves back toward the jet as the ratio is increased (Fig. 15b).

Heating augmentation results from the RCS roll jet interaction are shown in Fig. 16. In this case, the only active roll jet model piece was already coated with PSP and thus not visible. However, it is probably safe to assume that the immense cooling caused by the expansion of the jet would have been prevalent on the jet piece as well, overshadowing any heating caused by jet interaction on the surface. Similar to the PSP results, in this case, the greatest effect is seen when the $P_j/P_{T,2}$ is relatively large ($> \sim 200$). However, not enough data were collected to determine the actual value where the larger heating effect is seen. Furthermore, at the higher Reynolds number, the jet interaction at the surface actually decreases as the jet blowing pressure increases. Overall, the roll jet has a much greater effect on the surface than the yaw jet at all conditions, with maximum augmentation effect being greater than 10 at larger $P_j/P_{T,2}$, and approximately 6 when the $P_j/P_{T,2}$ value is less than 200.

Finally, TSP was applied to an aftbody configuration based on a preliminary design for the Orion vehicle. This design incorporated banks of roll and yaw jets (four of each) that were to be individually addressable. However, due to testing constraints, only one

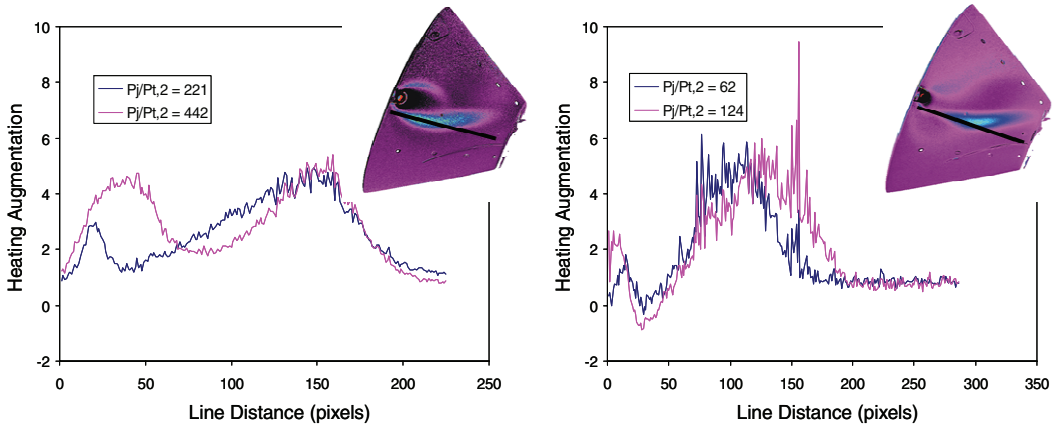

Fig. 15 Slices of the augmentation factors showing the effect of the yaw RCS jet. The insets show the approximate location of the slice. a) $Re = 5.9 \times 10^6$/m; b) $Re = 1.8 \times 10^6$/m.

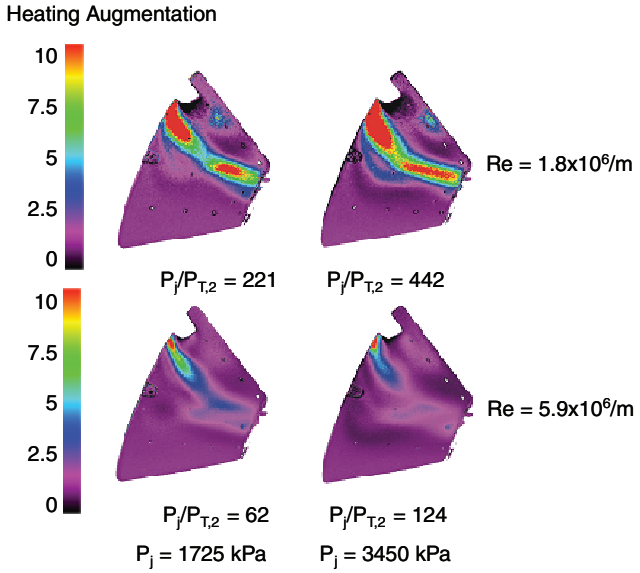

Fig. 16 Augmentation factors calculated for roll jet firing on the Apollo configuration.

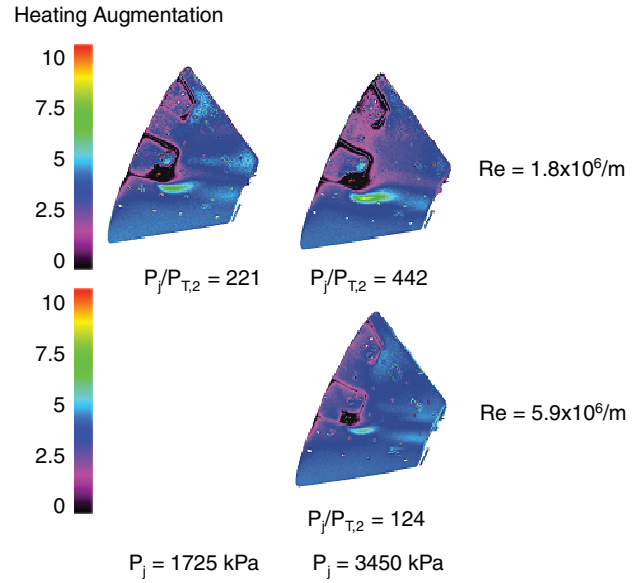

Fig. 17 Augmentation factors calculated for yaw jet firing on the Orion configuration.

configuration in which one of the yaw jets would fire was investigated. The augmentation results are shown in Fig. 17, and show that contrary to the Apollo configuration, the yaw jet shows little interaction with the surface from a heating standpoint. This is most likely due to the slightly different configuration of the jets (for this model, the jets blew outward more than the Apollo configuration). This decrease in intensity causes a significant decrease in the augmentation effect of the jet. The maximum augmentation occurs just aft of the jet exit (as is expected), but quickly decays probably due to the jet wash being entrained into the separation region. The maximum augmentation effect is approximately 2 and does not show appreciable dependence $P_j/P_{T,2}$.

V. Conclusions

The results from a series of proof-of-concept tests to assess the capability of PSP and TSP for hypersonic aerodynamics investigations have been presented. These tests were focused on visualizing and quantifying the interaction of RCS jets on the aftbody of capsule reentry vehicle shapes (a legacy Apollo-era model and a design based on the Orion). Careful experimental system design was needed for the PSP work, taking care to mitigate heating effects on the model surface that would overwhelm the extremely small pressure differences on the model. This was accomplished by coating the Apollo model surface with a thin layer of copper for use as a heat sink. In addition, the lifetime-based method of data acquisition was employed so that all data could be acquired quickly at condition. Using these techniques, the PSP was able to resolve the small pressure gradients on the model. However, existing pressure taps were needed to correct small temperature gradients that biased the data. Using these corrections, the PSP results agreed to within 10% of the measured pressure tap data. From these results, it was shown that the roll jet had much more interaction with the surface than the yaw jet, agreeing qualitatively with heating measurements previously performed on this shape.

TSP experiments were performed on noncopper coated models of both shapes. With the models constructed from an insulating material, most if not all of the heating effects were constrained to the surface. As this was the aftbody of the model, the temperature range measured was ideal for TSP. The temperature gradients were large enough to allow direct comparison of conditions using a "heating augmentation" factor. The TSP results agreed qualitatively with the PSP results and show that this technique could be a viable addition to existing thermographic phosphor coatings to measure aerodynamic heating effects, especially in areas where the temperature range is below the optimum operating range of the phosphor.

Acknowledgments

The authors would like to thank Anthony Robbins for providing support and coordination in the design and fabrication of the high-pressure system used for RCS jet simulation, and Kevin Hollingsworth, who, as principle facility engineer, was in charge of conducting the test and ensuring data quality.

References

[1] Buck, G. M., Watkins, A. N., Danehy, P. M., Inman, J. A., Alderfer, D. W., and Dyakonov, A. A., "Experimental Measurement of RCS Jet Interaction Effects on a Capsule Entry Vehicle," AIAA Paper 2008-1229, 2008.

[2] Kavandi, J., Callis, J., Gouterman, M., Khalil, G., Wright, D., Green, E., Burns, D., and McLachlan, B., "Luminescence Barometry in Wind Tunnels," *Review of Scientific Instruments*, Vol. 61, No. 11, 1990, pp. 3340–3347. doi:10.1063/1.1141632

[3] Morris, M. J., Benne, M. E., Crites, R. C., and Donovan, J. F., "Aerodynamic Measurements Based on Photoluminescence," AIAA Paper 93-0175, 1993.

[4] McLachlan, B., and Bell, J., "Pressure-Sensitive Paint in Aerodynamic Testing," *Experimental Thermal and Fluid Science*, Vol. 10, No. 4, 1995, pp. 470–485. doi:10.1016/0894-1777(94)00123-P

[5] Liu, T., Campbell, B., Burns, S., and Sullivan, J., "Temperature- and Pressure-Sensitive Luminescent Paints in Aerodynamics," *Applied Mechanics Reviews*, Vol. 50, No. 4, 1997, pp. 227–246.

[6] Liu, T., and Sullivan, J., *Pressure and Temperature Sensitive Paints (Experimental Fluid Dynamics)*, Springer–Verlag, Berlin, 2004.

[7] Hubner, J., Carroll, B. T., Schanze, K., and Holden, M., "Temperature- and Pressure-Sensitive Paint Measurments in Short-Duration Hypersonic Flow," AIAA Paper 99-0388, 1999.

[8] Nakakita, K., Yamazaki, T., Asai, K., Teduka, N., Fuji, A., and Kameda, M., "Pressure Sensitive Paint Measurement in a Hypersonic Shock Tunnel," AIAA Paper 2000-2523, 2000.

[9] Lakowicz, J., *Principles of Fluorescence Spectroscopy*, 2nd ed., Kluwer Academic/Plenum Publishers, New York, 1999, pp. 239–242.

[10] Engler, R., and Klein, C., "DLR PSP System: Intensity and Lifetime Measurements," *17th International Congress on Instrumentation in Aerospace Simulation Facilities*, IEEE, Piscataway, NJ, 1997, pp. 46–56.

[11] Holmes, J., "Analysis of Radiometric, Lifetime and Fluorescent Lifetime Imaging for Pressure Sensitive Paint," *The Aeronautical Journal*, Vol. 102, No. 1014, 1998, pp. 189–194.

[12] Bell, J. H., Schairer, T. E., Hand, L. A., and Mehta, R. D., "Surface Pressure Measurements Using Luminescent Coatings," *Annual Review of Fluid Mechanics*, Vol. 33, 2001, pp. 155–206. doi:10.1146/annurev.fluid.33.1.155

[13] Mitsuo, K., Egami, Y., Asai, K., Suzuki, H., and Mizushima, H., "Development of Lifetime Imaging System for Pressure-Sensitive Paint," AIAA Paper 2002-2909, 2002.

[14] Watkins, A. N., Jordan, J. D., Leighty, B. D., Ingram, J. L., and Oglesby, D. M., "Development of Next Generation Lifetime PSP Imaging Systems," *20th International Congress on Instrumentation in Aerospace Simulation Facilities*, IEEE, Piscataway, NJ, 2003, pp. 372–382.

[15] Buck, G. M., "An Imaging System for Quantitative Surface Temperature Mapping Using Two-Color Thermographic Phosphors," *34th International Instrumentation Symposium*, Instrument Society of America, Research Triangle Park, NC, 1988, pp. 655–663.

[16] Buck, G. M., "Surface Temperature/Heat Transfer Measurement Using a Quantitative Phosphor Thermography System," AIAA Paper AIAA-91-0064, 1991.

[17] Merski, N. R., "Global Aeroheating Wind-Tunnel Measurements Using Improved Two-Color Phosphor Thermography Method," *Journal of Spacecraft and Rockets*, Vol. 36, No. 2, 1999, pp. 160–170. doi:10.2514/2.3446

[18] Daryabeigi, K., "Global Surface Temperature/Heat Transfer Measurements Using Infrared Imaging," AIAA Paper 92-3959, 1992.

[19] Gallery, J., Gouterman, M., Callis, J., Khalil, G., McLachlan, B., and Bell, J., "Luminescent Thermometry for Aerodynamic Measurements," *Review of Scientific Instruments*, Vol. 65, No. 3, 1994, pp. 712–720. doi:10.1063/1.1145090

[20] Fey, U., Engler, R. H., Egami, Y., Iijima, Y., Asai, K., Jansen, U., and Quest, J., "Transition Detection Using temperature Sensitive Paint at Cryogenic Temperatures in The European Transonic Wind Tunnel (ETW)," *20th International Congress on Instrumentation in Aerospace Simulation Facilities*, IEEE, Piscataway, NJ, 2003, pp. 77–88.

[21] Hamner, M. P., Popernack, T. G., Jr., Owens, L. R., and Wahls, R. A., "Using Temperature Sensitive Paint Technology," AIAA Paper 2002-0742, 2002.

[22] Liu, T., Campbell, B. T., Sullivan, J. P., Lafferty, J., and Yanta, W., "Heat Transfer Measurement on a Waverider at Mach 10 Using Fluorescent Paint," *Journal of Thermophysics and Heat Transfer*, Vol. 9, No. 4, 1995, pp. 605–611. doi:10.2514/3.714

[23] Nakakita, K., Osafune, T., and Asai, K., "Global Heat Transfer Measurement in a Hypersonic Shock Tunnel Using Temperature-Sensitive Paint," AIAA Paper 2003-0743, 2003.

[24] Ohmi, S., Nagai, H., Asai, K., and Nakakita, K., "Effect of TSP Layer Thickness on Global Heat Transfer Measurement in Hypersonic Flow," AIAA Paper 2006-1048, 2006.

[25] Oglesby, D. M., and Upchurch, B. T., "In Pursuit of the Ideal Pressure Sensitive Paint," *7th Annual Pressure Sensitive Paint Workshop*, No. 1-3, Purdue University, West Lafayette, IN, 1999.

[26] Upchurch, B. T., Oglesby, D. M., and West, J. P., "New PSP Developments at NASA Langley Research Center—Low Temperature PSP," *6th Annual Pressure Sensitive Paint Workshop*, The Boeing Company, Seattle, WA, 1998.

[27] Asai, K., Amao, Y., Iijima, Y., Nishide, H., and Okura, I., "Novel Pressure Sensitive Paint for Unsteady and Cryogenic Wind Tunnel Testing," AIAA, Paper 2000-2527, 2000.

[28] Asai, K., Amao, Y., Iijima, Y., Nishide, H., and Okura, I., "Novel Pressure Sensitive Paint for Unsteady and Cryogenic Wind Tunnel Testing," *Journal of Thermophysics and Heat Transfer*, Vol. 16, No. 1, 2002, pp. 109–115. doi:10.2514/2.6658

[29] Egami, Y., Fey, U., and Quest, J., "Development of New Two-Component TSP for Cryogenic Testing," AIAA Paper 2007-1062, 2007.

[30] Micol, J. R., "Langley Aerothermodynamic Facilities Complex: Enhancements and Testing Capabilities," AIAA Paper 1998-0147, 1998.

[31] Carslaw, H. S., and Jaeger, J. C., *Conduction of Heat in Solids*, 2nd ed., Oxford University Press, London, 1959.

[32] Fay, J. A., and Riddell, F. R., "Theory of Stagnation Point Heat Transfer in Dissociated Air," *Journal of the Aeronautical Sciences*, Vol. 25, No. 2, 1958, pp. 73–85.

[33] Hollis, B. R., "Real-Gas Flow Properties for NASA Langley Research Center Aerothermodynamics Facilities Complex Wind Tunnels," NASA CR 4755, Sept. 1996.

[34] Jones, R. A., and Hunt, J. L., "Effects of Cavities, Protuberances, and Reaction-Control Jets on Heat Transfer to the Apollo Command Module," NASA TM X-1063, March 1965.

A. Naguib
Associate Editor